

18  
MAR 27 1939  
L. M. a-L.

115.54  
MAR 27 1939  
L. M. a-L.  
SR/1

TECHNICAL MEMORANDUMS  
NATIONAL ADVISORY COMMITTEE FOR AERONAUTICS

Copy  
~~\_\_\_\_\_~~

\_\_\_\_\_  
No. 890  
\_\_\_\_\_

EXPERIMENTS ON A SLOTTED WING

By P. Ruden

Deutsche Luftfahrtforschung  
Jahrbuch 1937  
Verlag von R. Oldenbourg, München und Berlin

**FILE COPY**

To be returned to  
the files of the Langley  
Memorial Aeronautical  
Laboratory.

1.2.2.3.1  
1.2.1.4.3

Washington  
March 1939



3 1176 01440 6657

NATIONAL ADVISORY COMMITTEE FOR AERONAUTICS

TECHNICAL MEMORANDUM NO. 890

EXPERIMENTS ON A SLOTTED WING\*

By P. Ruden

The results of pressure distribution measurements that were made on a model wing section of a Fieseler F 5 R type airplane are presented in this report. Comparison of these model tests with the corresponding flight tests indicates the limitations and also the advantages of wind tunnel investigations, the advantages being particularly that through the variety of measuring methods employed the more complicated flow conditions may also be clarified. A fact brought out in these tests is that even in the case of "well rounded" slots it is possible for a vortex to be set up at the slot entrance and this vortex is responsible for certain irregularities in the pressure distribution and in the efficiency of the slot.

I. INTRODUCTION

The tests were conducted at the instigation of the DVL, which for its part carried out pressure-distribution measurements in flight on a wing section of the Fieseler F 5 R type airplane. By parallel tests in the wind tunnel it was intended to obtain new data on the question of the applicability of wind-tunnel measurements to full-scale conditions. In addition, wind-tunnel investigations appeared particularly well suited to clarify the flow phenomena in the wing slot. The interpretation of the pressure-distribution measurements, however, although supplemented by boundary-layer investigations, was so difficult that it was necessary to render the flow visible. The simplest method that at first suggested itself was that of observing the water flow in an open channel in which a wooden model of the slotted wing was placed. Unfortunately, this method proved quite inadequate, since, in order to maintain the Reynolds Number as large as possible, higher flow speeds were required than those normally employed. With such high speeds, however, the disturbances

---

\*Versuche an einem Düsenflügel." Jahrbuch 1937 der deutschen Luftfahrtforschung, pp. I 76-86.

due to the surface waves in the slot become so strong that the surface condition no longer reflects the true picture of the corresponding air flow. Reliable results can be obtained only by means of underwater-flow pictures, although in this case it is not quite possible to attain the Reynolds Number of the wind-tunnel tests; because of illumination difficulties encountered.

## II. PROCEDURE IN WIND-TUNNEL TESTS

Since the primary object of the wind-tunnel investigations was the comparison with the DVL flight tests, the pressure-distribution measurements were made on a model wing of the Fieseler F 5 R type airplane already mentioned, only the left half-wing reduced to the scale 1:5 being employed. This half-wing could be mounted as a cantilever wing on a rotating circular end plate of plywood with the prescribed dihedral in the free jet of the tunnel (fig. 1). The wing section at which the pressure distribution was measured with the aid of pressure orifices was the same as that employed in the DVL flight tests. The profile section is shown in figure 2, the hinge axis of the flap being indicated. Figure 2 likewise shows the position of the pressure orifices. Although an attempt was made to obtain a large number of pressure orifices in the slot, it was not possible for lack of space to bore orifices in the neighborhood of the flap nose. For the same reason, it was necessary to dispense with an orifice on the upper surface at the trailing edge of the main wing.

The tests were conducted at a wind velocity of 34.8 m/s (78 m.p.h.). The Reynolds Number based on the chord of the section  $t = 292.8$  mm was about  $7 \times 10^5$ . The aileron always remained in the undeflected position, the flap setting  $\beta$  and the angle of attack  $\alpha$  being varied. The angle  $\alpha$  is the geometric angle of attack (without wind-tunnel correction) taken with respect to the direction of the reference axis (fig. 2). The flap settings were taken to be  $\beta = 0^\circ, 10^\circ, 19^\circ, \text{ and } 34^\circ$ . (In the DVL measurements, the settings were  $0^\circ, 19^\circ, \text{ and } 32^\circ$ .)

The angle-of-attack range investigated embraced the two separation ranges. Since it was first assumed that within the range of "adhering flow" the pressure curve taken as a function of the angle of attack at any measuring point would show no irregularities, the relatively

large angle-of-attack interval of about  $6^\circ$  was chosen and this was reduced to about half only in the neighborhood of the separation ranges. On evaluating the results, it was found, however, that the expectations entertained with regard to the smoothness of the pressure curves were in no way fulfilled. In order to check this result, subsequent measurements were made at  $\beta = 34^\circ$  for additional angles of attack.

The extrapolation of the pressure-distribution curves from pressure orifice 9 down to the trailing edge of the main wing presents great uncertainty. For this reason, pressure measurements for several combinations of  $\alpha$  and  $\beta$  were made along the upper surface of the main wing down to the trailing edge with the aid of a fine static tube. At those positions where the surface pressures could be determined in the usual manner, the reliability of this method could be checked by comparison. It turned out, as was also expected, that the measuring accuracy of the static tube in the immediate neighborhood of the wing surface was unsatisfactory, but nevertheless did give a correct indication of the general tendency of the pressure diagram.

Finally, with the aid of a fine Brabbée tube of about 0.8 mm outside diameter, the distribution of total pressures was measured in a normal section close behind the slot outlet for a flap setting of  $34^\circ$ . Since the wing changes its attitude somewhat with the wind, on as compared with its attitude in quiet air it was necessary for the distance of the tube from the wing to be determined during the measurement itself. This could be done in a relatively simple manner by determining the position of smallest total pressure behind the main wing trailing edge with the greatest possible accuracy. Before each measurement the total pressure tube was adjusted to the mean flow direction with the aid of a streamer. Since with fixed angle of attack and flap deflection, appreciable changes in flow directions are not likely to arise within the boundary layer and the slot and since the Brabbée tube is very insensitive to changes in direction, this method of adjusting the total pressure tube in the flow direction appeared sufficiently accurate. Check tests with somewhat varied tube directions showed in fact that the measurements were excellently reproducible.

## III. PRESSURE DISTRIBUTIONS

The results of the pressure-distribution measurements are contained in tables 1 to 4. The pressures at the surface are expressed in fractions of the dynamic pressure  $q$  corresponding to the tunnel velocity. The intermediate measurements mentioned above are not indicated. Figures 3 to 6 show as examples the pressure distribution diagrams for  $\beta = 0^\circ$  and  $\beta = 34^\circ$  plotted against the reference axis of the wing section. For  $\beta = 34^\circ$  the plots are presented in such a manner as if the flap were rotated backward from its zero position, this manner of presentation adding to the clearness of the diagram.

The pressure-distribution curves shown are generally somewhat uncertain at their sharpest maxima since no measurements were actually made at the corresponding positions. Thus, for example, the peak on the upper surface at the wing leading edge is seldom accurately known, although it is just in this region that the orifices are most closely spaced. On the upper surface of the main wing similar difficulties are encountered in the neighborhood of the trailing edge, particularly since space limitation prevented installation of a pressure orifice here.

For  $\beta = 0^\circ$  the entire appearance of the pressure-distribution curve indicates that at this position, the pressure on the suction side of the main wing passes over smoothly into the pressure at the suction side of the flap. This would also follow from the fact that the slot outlet is nearly closed for  $\beta = 0^\circ$ . For greater flap settings, this, however, is no longer the case. The fact that the dotted peaks arise in this case was already shown by the above-mentioned qualitative measurements with the static tube.

For  $\beta = 0^\circ$  the slot, as mentioned above, was almost closed. In the pressure distribution this shows up in the value the pressure assumes in the entire slot, the value being that which is attained at the lower side of the section at the inlet to the slot, and in the discontinuous change which the pressure undergoes both on the upper side of the flap as well as at the trailing edge of the main wing in the passage through the slot outlet. This discontinuity is indicated in the pressure-distribution curves (figs. 3 and 4) by the two closely lying vertical lines. At the lower left edge of these vertical lines, the pres-

sure curves include a doubly enclosed region, which does not, however, contribute anything in the integration, since it must be traversed once in one direction and then in the reverse direction. If this doubly enclosed region is neglected, the pressure distribution for  $\alpha > 7.6^\circ$  barely differs from those of a corresponding simple section. In the case of small negative angles of attack, however, there is a definite disturbance on the lower surface, which shows up in the fact that there is a greater pressure rise at the leading edge of the flap on the upper surface than on the lower surface.

As examples of the pressure-distribution diagrams that are obtained with open slot, there are shown the pressure-distribution curves for  $\beta = 34^\circ$  (figs. 5 and 6). The characteristic phenomena show up most clearly in this case. For large negative angles of attack, the flap lies almost completely in the wake region of the main wing. The flap pressure distribution is correspondingly distorted. Since the air which flows past the flap consists of the small energy content boundary layer, the full dynamic pressure ( $p/q = 1$ ) is not attained at the stagnation point, which, on account of the division of the flow, must necessarily lie in the neighborhood of the flap nose. This pressure is first attained for  $\alpha \geq -7.4^\circ$ . The maximum pressure on the flap upper surface at first rapidly increases with increasing  $\alpha$  up to  $\alpha = 1.6^\circ$  and then drops again to a constant value between  $\alpha = 7.6^\circ$  and  $16.7^\circ$ . In the angle-of-attack range  $1.6^\circ \leq \alpha \leq 16.7^\circ$ , the pressure rise along the upper surface of the flap is satisfactory. At  $\alpha = 19.7^\circ$ , the maximum negative pressure on the upper surface of the flap drops rather abruptly. The flow separates and thereby initiates separation also on the upper surface of the main wing. The pressure changes here described can be conveniently followed with the aid of figure 7 where the pressures at each of the pressure orifices have been plotted as functions of the angle of attack. The most important result established is the following: For a given flap setting and given dynamic pressure corresponding to the tunnel velocity, the largest negative pressures at the flap nose occur at a small angle of attack, corresponding to high-speed flight. The flap nose may thus, under certain circumstances, experience unusually high stresses.

## IV. THE FLOW PAST THE SLOT

Considered from the physical point of view, the lowering of the negative pressure peaks on the upper surface of the flap in the angle-of-attack range  $1.6^\circ \leq \alpha \leq 7.6^\circ$  is particularly striking. Considering the pressures at orifices 10 to 13 lying at the slot inlet on the under surface of the main wing, there is an even more remarkable sudden change observed in the above-mentioned angle-of-attack range. Whereas, for  $\alpha = 1.6^\circ$  at the slot side of the main wing, an initial drop in pressure is followed by a rather strong pressure rise (fig. 5), for  $\alpha = 7.6^\circ$ , these pressure fluctuations no longer occur (fig. 5). The reason for the pressure changes indicated above for  $\alpha = 1.6^\circ$  becomes clear if it is assumed that a vortex is built up at the slot inlet as sketched on figure 12a. Since the vortex contains only the boundary-layer air, the value  $p/q = 1$  is not attained at the stagnation point behind the vortex. At larger angle of attack the vortex completely disappears for  $\beta = 34^\circ$ .

That quite similar phenomena occur for other flap deflections,  $\beta = 10^\circ$  and  $19^\circ$ , is shown by figures 8 and 9. In these the pressure distribution curves have been collected for all of the values of  $\beta$  investigated (with the exception of  $\beta = 0^\circ$ ) and for  $\alpha = 1.6^\circ$  and  $\alpha = 7.6^\circ$ . The only difference that occurs for  $\beta = 10^\circ$  and  $19^\circ$  as compared with the case previously discussed for  $\beta = 34^\circ$  is in the fact that the slot vortex apparently does not quite disappear at the higher angles of attack but only becomes smaller. This may be accounted for by the fact that the flow through the slot at the smaller flap deflections is throttled considerably more at the narrow outlet of the slot than at  $\beta = 34^\circ$ .

In order to prove the actual existence of the vortex at the slot inlet, pictures of the flow through the slot were obtained in a water channel. After several preliminary tests it was found to be necessary to abandon the usual method of surface pictures and conduct the tests in a closed channel having a flow cross section of  $250 \times 500$  mm<sup>2</sup>. The model of the slotted wing had a chord of 200 mm and a span of 250 mm; i. e., it extended from one wall to the other. The airfoil section was the same along the entire span. The middle plane of the channel was illuminated with the aid of two arc lamps the paths of whose rays were concentrated on the plane by cylindrical lenses.

Particles that were suspended in the water ahead of the model wing reflected the light in this plane and traced the flow paths. Since with the existing illumination apparatus, it was necessary to employ particles with as good reflecting ability as possible, aluminum powder that was usually used in the surface pictures was again employed. The difficulty of making the aluminum powder remain suspended under the water was overcome by adding alcohol to the powder. With this addition, the favorable condition was simultaneously obtained of reducing the total weight of the suspended particles to such an extent that a large part of the aluminum powder could remain suspended in a water-filled stand cylinder without appreciable sinking velocity.

The flow through the slot thus rendered visible in the manner described above was photographed. Particularly beautiful pictures from which quantitative results could also be also be derived were obtained when a rapidly rotating diaphragm, which broke up the streamline picture evenly, was mounted in front of the camera objective. Figure 10 shows one such photograph obtained. In the corresponding test the flow velocity of approach was somewhat above 1 m/s (2.24 m.p.h.), the Reynolds Number referred to the model chord being about  $2 \times 10^5$ . The model wing profile agreed in outer contour with that shown in figure 2. The slot inlet, however, even in the preliminary tests was widened. The vortex at the entrance in this case, even for the relatively large angle of attack of  $4^\circ$ , is very clearly shown. The flap deflection was  $10^\circ$ .

In the preliminary tests, which were also conducted with the slot shape of figure 2, it was found that the vortex practically disappeared at larger values of  $\alpha$ . The corresponding photographs are unfortunately unsuited for reproduction.

There is still to be considered the question whether the vortex occurs also at larger Reynolds Numbers. For the Reynolds Number of the wind tunnel its existence is assured by the measured pressure distribution. Whether it exists at much higher Reynolds Number can only be established by further tests.

In order to investigate somewhat more closely the effect of the vortex on the flow past the slot, total pressure measurements were made close behind the slot exit during the wind-tunnel tests on the model wing of the F 5 R

airplane. The flap setting  $\beta$  was again  $34^\circ$ . Figure 11 shows the results of this investigation. The height of the total pressure peak suffers the same fluctuations as the negative pressure peak of the flap upper surface. At large negative angles of attack the energy of the flow through the slot is small. The loss is a result of the adverse pressure gradient, which the boundary layer at the under side of the section must overcome in its path from the main wing nose to the slot inlet (see fig. 5,  $\alpha = -13.5^\circ$  to  $-4.4^\circ$ ). With increasing angle of attack the adverse pressure gradient becomes smaller and the total pressure maximum at the slot exit as well as the negative pressure peak at the flap upper surface increase in height in about the same ratio in which the pressure gradient decreases. Simultaneously the vortex at the slot inlet is built up as shown by the pressure distribution at the inlet. In a remarkable manner the total pressure and negative pressure peaks attain their maximum values precisely when the pressure distribution curves indicate the most marked formation of the vortex, namely at the angle of attack  $\alpha = 3^\circ$ . With increasing angle of attack the height of the total pressure peak decreases very rapidly and then slowly again increases. The negative pressure peak on the flap upper surface also begins to decrease immediately above  $\alpha = 3^\circ$  but does not increase again after that. Figure 11 ( $\alpha = 4.3^\circ$  to  $16.3^\circ$ ) provides a simple explanation for this. The boundary layer from the main wing upper surface increases in thickness with increasing  $\alpha$ , so that the energy transported to the slot is still just sufficient to hold the negative pressure and the stream deflection connected with it to a constant height. After the boundary-layer thickness has exceeded a certain value (at  $\alpha = 17^\circ$ ) the energy of the slot flow is no longer sufficient to prevent separation. It is not yet possible to predict how great this thickness must be for a given profile section and given energy of slot flow. The determination of this critical boundary layer-thickness is an urgent problem in slotted-wing investigation.

The lowering of the total pressure peak in the slot outlet above  $\alpha = 3^\circ$  is evidently connected with the vanishing of the slot vortex. It might be expected that with the disappearance of the vortex there will necessarily be a considerable increase in the energy of the slot flow, more particularly since the boundary layer on the under surface of the main wing has only a small pressure gradient to overcome, but on the contrary with increasing angle of attack undergoes stronger accelerations. The measurements show

the contrary to be true, however, at least for the angle of attack range immediately above  $3^\circ$ . The explanation of this apparent contradiction probably lies in the stabilizing effect the centrifugal forces are known to have in the neighborhood of a convex wall (reference 1). As may be seen from figure 12, the curvature of the streamlines at the slot inlet is much greater in the presence of a vortex than when it is absent. Correspondingly the centrifugal effects in the first case are much greater than in the second.

Fluid particles from the boundary layer and therefore possessing widely varying absolute velocities are also acted upon by centrifugal forces of various magnitudes for streamlines of approximately equal curvature, the slower particles by smaller, and the faster particles by larger forces. The former may in a given case be drawn into the vortex toward the region of lower pressure directed inward. This action delays turbulent mixing of the boundary-layer particles with the flow process, which is always associated with energy losses. At the second curvature of the streamlines behind the vortex stagnation point S, the velocities and hence also the centrifugal forces are small on account of the nearness to the stagnation point. The streamline curvature at this position would tend to promote the mixing, as may be seen after some consideration but for the reasons given, however, can have no important effect on the mixing, particularly since the slowest particles have already wandered off into the vortex region. The effect of this centrifugal action is clearly brought out in the form of the total pressure peaks for  $\alpha = -1.9^\circ$  to  $+3^\circ$  in figure 11. The turbulent mixing is so slight that the shape of the boundary layer of the lower surface may be recognized only at the slot outlet. After the vortex vanishes, the curvature of the streamlines at the slot inlet becomes less. At the same time the velocities decrease on account of the increasing opposing pressure gradient. The result is that the stabilizing effect of the centrifugal force at this position becomes too weak to prevent turbulent mixing. On the other hand, no stagnation point is built up within the slot at the position of second curvature previously mentioned, so that the centrifugal effects on account of the high flow velocities occurring there become greater and may support the turbulent mixing. This is shown both in the shape and in the height of the total pressure peaks for  $\alpha > 3.7^\circ$ .

The explanation here given of the slot flow has not

gone into a thorough description of the processes involved. It was nevertheless presented with sufficient detail, since it appeared important to show clearly with the aid of an example the many aspects of the problems connected with the slotted wing and thus provide starting points for the indispensable detail investigations. The fact that even for slots given as "well rounded" a vortex is set up at the entrance is not only interesting in itself but will lead to a study of what shape the slot should be given in order that such a vortex formation may be avoided. As is shown on figure 10, a flattening of the slot inlet should have no favorable effect. On the contrary, a slot inlet of still greater curvature as shown in figure 2 should be better. It is to be observed that the shape of a good slot inlet certainly depends also on the width of the slot at the exit and hence on the amount of throttling. Since there is a steady flow of new air from the boundary layer to the vortex, there must necessarily occur a throwing off of vortex material. With this process are associated periodic pressure fluctuations. Their frequency appears to lie so high, however, that they are not likely to give rise to flutter. It is possible, however, that the undesirable vibrations of the ailerons, which are sometimes observed with slotted wings, may be connected with these frequencies. No systematic explanation has as yet been given of the question as to what extent the flow resistance through the slot is affected by the vortex formation. In the treatment of all these questions, there must also naturally be taken into account the questions of control surface balance.

## V. THE SEPARATION PROCESS

For the sake of completeness of the discussion of the pressure-distribution curves, there will be given a short description of the separation process. The highest measured negative pressure peaks in the neighborhood of the nose of the airfoil are given in table 5. The absolute numerical values increase with  $\beta$  (except for  $\beta = 34^\circ$ ). They show clearly how the upper surface boundary layer is made capable of overcoming a large pressure gradient through the energy in the slot, which increases with  $\beta$ .

Table 5

$\beta$	$(p/q)_{\min}$
0°	-4.40
10°	-4.70
19°	-5.35
34°	-5.31

In the separation process, two stages may be recognized:

1. The separation proceeds from the trailing edge of the section forward without, however, reaching the airfoil nose. This shows up in the smaller negative pressures in the separation zone. At the nose a negative pressure peak is maintained.
2. Complete separation of the flow on the upper surface - the negative pressure peaks on the upper surface vanishing.

In the first stage an important difference arises on the one hand for  $\beta = 0^\circ$  and  $10^\circ$ , and on the other hand for  $\beta = 19^\circ$  and  $34^\circ$ . Whereas, in the first case, the separation point shifts rather steadily from the trailing edge forward, in the second case the separation occurs much more violently. At negative angles of attack the two stages in the flow separation are not so clearly discernible.

## VI. INTEGRATION OF PRESSURE-DISTRIBUTION CURVES

It will be assumed in what follows that the  $x$  and  $y$  axes are as indicated in figure 2 and remain fixed to the main wing. When the flap is deflected by an angle  $\beta$ , the  $x$  and  $y$  coordinates of the pressure orifices which lie on the main airfoil remain unchanged while those on the flap change their coordinates. Plotting the measured pres-

sures against the  $x$  and  $y$  axes, respectively, the normal and tangential force coefficients may be determined by integration. By using the integration, there is at the same time obtained the pitching-moment coefficient with respect to the origin of coordinates  $O$  (fig. 2). We have

$$c_n = \int_{1,2} \left( \frac{p}{q} \right) d \left( \frac{x}{t} \right) \quad c_t = \int_{1,2} \left( \frac{p}{q} \right) d \left( \frac{y}{t} \right)$$

$$c_m = \int_{1,2} \left( \frac{p}{q} \right) \left( \frac{x}{t} \right) d \left( \frac{x}{t} \right) + \int_{1,2} \left( \frac{p}{q} \right) \left( \frac{y}{t} \right) d \left( \frac{y}{t} \right) *$$

The reference length  $t$  is the chord of the wing section,  $c_n$  and  $c_t$  are positive in the positive direction of the  $y$  and  $x$  axes, respectively, and  $c_m$  is positive for a nose-heavy moment. In the integration, the pressure distribution of the main airfoil (subscript 1) and that of the flap (subscript 2) are to be integrated separately. The accuracy of the coefficients thus obtained depends naturally very much on the reliability with which the points have been obtained for the corresponding pressure distribution. The  $c_t$  values are therefore relatively uncertain, since in the plot against  $y$  the contour of the nose of the airfoil becomes of great importance and with the large changes in pressure occurring at that position the existing number of pressure orifices is by no means sufficient. The above-mentioned lack of sufficient information on the pressure variation at the main airfoil nose shows up to the greatest extent in the determination of the pitching-moment coefficient principally in the first integral. The contribution of the second integral is always relatively small, although by no means negligible since it may amount to 5 percent of the value of the first integral. Aside from the above-mentioned uncertainties, the values of the coefficients obtained through integration of the pressure distribution curves cannot fundamentally correspond with those obtained by force measurements, since the effect of the skin friction is neglected.

---

\*The relation between the coordinates  $x$  and  $y$  and the coordinates  $X$  and  $Y$  indicated in figure 2 is given by

$$X = \frac{x}{t} 100, \quad Y = \frac{y}{t} 100.$$

The values of the coefficients  $c_n$ ,  $c_t$ , and  $c_m$  given by integration of the pressure-distribution curves are given at the heads of tables 1 to 4, and are plotted in figures 13, 14, and 16 as functions of the angle of attack. The curves of  $c_n$  against  $\alpha$ , except for the stalling ranges, show the usual approximately linear relation. For positive  $c_n$  the critical angle of attack at which separation begins becomes smaller as the flap deflection  $\beta$  becomes larger. For negative  $c_n$  the reverse is the case. Figure 14 shows how the coefficient  $c_t$  becomes unfavorable with increasing  $\beta$ , since the drag becomes greater, the greater the value of  $c_t$  becomes. On the  $c_t$  curves, moreover, the two stages of separation are clearly evident. The value of  $c_t$  increases in two relatively sharp jumps, the first of which, at  $\beta = 19^\circ$  and  $34^\circ$ , is much greater than that at  $\beta = 0^\circ$  and  $10^\circ$ . This corresponds to the fact brought out in the previous section that the first stage of the separation process in the case of the first pair of flap deflections sets in much more violently than in the case of the second pair. Figures 13 and 14 also indicate the proportion of the contributions of main airfoil and flap. Particularly striking is the fact that  $c_{n_2}$ , the normal force coefficient of the flap, is practically constant. The increasing reduction in  $c_t$  with increase in  $\beta$  is brought about exclusively by the flap. In the value of  $c_{t_2}$ , the tangential force coefficient of the flap, there also enters (for  $\beta = 19^\circ$  and  $34^\circ$ ) the drag increasing effect of the slot vortex.

From the values of  $c_n$  and  $c_t$  there were computed (without wind-tunnel correction, however) the values of the lift and drag coefficients  $c_a$  and  $c_w$ , plotted as polars in figure 15. The increase in drag with increasing flap deflection is particularly evident.

Whereas the processes which may be associated with the appearance of the slot vortex do not show up in the normal force coefficient  $c_n$ , they do show up very clearly in the values of  $c_m$  (fig. 16). The slope  $dc_m/d\alpha$  is noticeably changed in the angle of attack range  $3^\circ < \alpha < 8^\circ$ . For  $\beta = 34^\circ$ , the curve  $c_m$  is drawn through a particularly large number of test points that were subsequently obtained.

## VII. COMPARISON OF WIND TUNNEL MEASUREMENTS

## WITH THE RESULTS OF THE FLIGHT TESTS

An entirely satisfactory comparison of both these sets of measurements is not simple. This is first of all due to the difficult conditions under which it was necessary to carry out the flight tests. The number of pressure orifices could not be made as large as would be necessary for an entirely reliable determination of the pressure distribution. At the main wing trailing edge from  $X = 60.0$  on, there were no pressure orifices. In the case of the model wing, there were in this region the four orifices 9 to 12. In addition to the difficulty of obtaining an approximately correct pressure distribution in this region, however, it was necessary, in evaluating the flight test results, to fair the curves arbitrarily at these positions, particularly since the supplementary qualitative measurements with the static tube that were found useful in the wind tunnel tests were not available. Moreover, the pressure orifices at the airfoil nose in the flight tests were not as numerous as in the wind-tunnel tests. In the DVL tests, the first pressure orifice was located at  $X = 2.5$ , while in the wind-tunnel test orifice 1 was at  $X = 0$ , orifice 2 at  $X = 2.22$ , and orifice 17 at  $X = 2.56$ . At the airfoil nose the stagnation point and the maximum negative pressure position are close beside each other. With increasing distance from the airfoil nose, the pressure differences between the upper and lower surfaces rapidly decrease. It was, therefore, to be expected that the DVL tests would give smaller resultant pressures than the model tests. A particular difficulty encountered was the fact that in the flight tests it was necessary for practical reasons to connect up the pressure orifices on the upper and lower surfaces with each other. If the pressures are measured individually as was the case in the model tests, the stagnation point at the nose of the airfoil can be given with relative accuracy if at no pressure orifice the value  $p/q = 1$  is attained. For the method of measurement used in the DVL test, however, this was not longer possible.

On the other hand, on account of the small dimensions of the model, the model test had the disadvantage that complete geometric similarity, in spite of all care taken, could hardly be attained. The slot lip of the model was particularly difficult to construct, since the main airfoil trailing edge ends very sharply and for reasons of strength the model thickness could not go below a certain limit. It

is also very difficult to reproduce the shape of the airfoil nose with the required accuracy when it is considered that it is at this position that the pressure is extremely sensitive to the smallest changes in shape (reference 2).

With the above considerations in mind, no too strict rule should be applied for the comparison of the pressure distributions. Actually, for example, according to figure 17, large differences arise at the airfoil nose at  $\beta = 0^\circ$ . For comparison, the pressure distributions for the same value of  $c_n$  were drawn above each other. The curves of the flight measurement are interpolated from the values given by Kiel (reference 3) while the resultant pressure for the model test had to be read off from the drawn pressure distribution curves. On account of the steep slope of the pressure curves at the airfoil nose, the pressure difference of two points lying above each other is never uniquely determined, since there is a chance for large discrepancies in the measurements. Only for the larger values of  $x$  does the determination of the pressure differences become to some extent reliable.

The curves for  $\beta = 0^\circ$ ,  $c_n = 0.60$  (fig. 17) are particularly interesting. The stagnation point obviously remains undetermined on the curve corresponding to the flight measurement. In figure 3 for the corresponding pressure-distribution curve  $\beta = 0^\circ$ ,  $\alpha = 7.6^\circ$ , the test points which would correspond to the first two pressure orifices of the flight measurements are indicated by large crosses. Their position confirms what was said. The same applies to the other curves of figure 17. From the pressure distributions of figure 4 for  $\beta = 0^\circ$ ,  $\alpha = 16.7^\circ$  ( $c_n = 1.18$ ) and  $\alpha = 19.7^\circ$  ( $c_n = 1.26$ ) there may be determined the resultant pressure which corresponds to the first two pressure orifices of the DVL test and thus show that the stagnation point and maximum negative pressure are both undetermined. At a greater distance from the airfoil nose, the agreement between the wind-tunnel measurement and the flight tests is surprisingly good, although the error made in drawing the pressure distribution curves enters the value of  $c_n$  and equal  $c_n$  values were chosen as a basis for comparison.

The comparison of the resultant distributions for  $\beta = 19^\circ$  also shows quite satisfactory agreement for  $c_n = 1.15$ , 1.55, 1.80. An exception must here be made naturally for the differences at the airfoil nose for which the explanation may again be found in the measured pressure distributions in the wind tunnel. There may be observed here the additional small peak at the main airfoil trailing edge. The flight test provided no test points for the pressure distribution for this region since, as already mentioned,

there were no pressure orifices at the main airfoil trailing edge. From the comparison of the pressure-difference curves it was found that the value of  $c_n$  given by Kiel is somewhat too small, since his curves drop too sharply at the main airfoil trailing edge. The curves of figure 18 show the greatest additional peak for  $c_n = 0.75$ . For this reason the agreement of the continuous and dotted curves in this case is here also the least favorable. If, however, the value of 0.66 given by Kiel is used, the agreement, except for the main wing trailing edge, is again very good.

Figure 19 gives the values obtained by integration of the flight measurements and the wind-tunnel measurements for  $\beta = 0^\circ$  and  $19^\circ$ . Even taking into account the fact that in the case of the model wing the flow separation occurs much earlier than in the full-scale wing, the agreement is nevertheless satisfactory. The fact that the points with reference to which the pitching-moment coefficients were obtained were somewhat different is not particularly important. A recomputation of the wind-tunnel results using the reference point of the DVL measurements, which point coincides approximately with orifice 1 (fig. 2) gives only a slight shift in the values. It will be seen, however, that the moment coefficients of the flight test are greater for  $\beta = 0^\circ$  and smaller for  $\beta = 19^\circ$ . It should be remarked that for  $\beta = 19^\circ$  the resultant pressure distributions given by Kiel necessarily yield a smaller pitching-moment coefficient since the omitted smaller pressure peak at the main airfoil trailing edge exerts an appreciable effect on account of the large lever arm.

Summarizing, it may be stated that the wind-tunnel tests give quite reliable results in the prestalling range\* but that the separation of the flow occurs much earlier than in the full-scale tests. If it is assumed that the maximum value of  $c_n$  attained in flight also agrees approximately with the corresponding value of the wing section investigated, the result is obtained that the maximum normal force coefficient determined in the wind tunnel is exceeded in flight by 0 to 25 percent. (see fig. 20). Aside

---

\*It must be expressly emphasized, however, that the deviations in the pressure curves shown in figures 17 and 18 in the neighborhood of the airfoil nose may, with great probability, be considered as accidental and further tests are required for confirmation.

from the fact that the maximum  $c_n$  value corresponding to the measuring section of the flight test is probably higher than the one here assumed, the comparison given in figure 20 is not entirely free from objection, since in the flight test the propeller slipstream has a stabilizing effect on the air flow while in the wind-tunnel test separation of the flow was promoted by the boundary layer of the end plate.

### VIII. SUMMARY

The results of wind-tunnel tests on a slotted wing are presented, the object of the investigation being the determination of the pressure distributions on a wing section with flap. The model was that of a wing of a Fieseler F 5 R type airplane. For studying the flow phenomena in the slot, total pressure measurements were taken in the boundary layer behind the slot exit and the flow in the slot of a similar wing section rendered visible in a water channel. The attempt to furnish a physical explanation of the slot flow and its effect on the pressure distribution raises a number of questions whose answers will have to be provided by further slotted-wing investigations.

Comparison of the wind-tunnel measurements with the corresponding flight tests conducted by the DVL showed that the wind-tunnel results could be reliably applied to full-scale conditions as long as the below-stalling range is considered, but that the maximum value of the normal force coefficient of the wind-tunnel measurement is from 0 to 25 percent below the value attained in the flight test.

Translation by S. Reiss,  
National Advisory Committee  
for Aeronautics.

## REFERENCES

1. Betz, A.: Über turbulente Reibungsschichten an gekrümmten Wänden. Vorträge aus dem Gebiete der Aerodynamik und Verwandter Gebiete, Aachen, 1929, pp. 10-18.
2. Betz, A.: Modification of Wing-Section Shape to Assure a Predetermined Change in Pressure Distribution. T.M. No. 767, N.A.C.A., 1935.
3. Kiel, Georg: Pressure Distribution on a Wing Section with Slotted Flap in Free Flight Tests. T. M. No. 835, N.A.C.A., 1937.

Table 1. Flap deflection  $\beta=0^\circ$ .

$\alpha^\circ$	-16,5	-13,5	-10,4	-7,4	+1,6	+7,6	+13,7	+16,7	+19,7	+21,0	+22,7	+24,6	+25,7
$c_n$	-0,67	-0,70	-0,66	-0,49	+0,19	+0,60	+0,99	+1,18	+1,26	+1,33	+1,28	+1,22	+0,92
$c_t$	+0,09	+0,07	0	-0,02	+0,01	-0,05	-0,16	-0,22	-0,28	-0,29	-0,27	-0,26	0
$c_m$	-0,25	-0,24	-0,16	-0,11	+0,04	+0,15	+0,25	+0,30	+0,35	+0,39	+0,41	+0,41	+0,33
Orifice location no.	$\frac{P}{q}$												
1	-0,66	-0,68	-1,45	-1,05	+0,85	+0,65	-0,75	-1,87	-2,91	-3,33	-3,52	-3,83	-0,82
2	+0,92	+0,89	+0,91	+0,84	+0,04	-1,00	-2,39	-3,17	-3,91	-4,39	-4,38	-4,40	-0,92
3	+0,66	+0,60	+0,59	+0,45	-0,38	-1,17	-2,15	-2,67	-2,81	-2,91	-2,72	-2,61	-0,86
4	+0,42	+0,35	+0,32	+0,19	-0,57	-1,21	-1,96	-2,29	-2,42	-2,49	-2,24	-2,04	-0,82
5	+0,15	+0,09	+0,05	-0,06	-0,69	-1,16	-1,70	-1,85	-1,95	-1,96	-1,65	-1,35	-0,78
6	-0,05	-0,10	-0,11	-0,21	-0,67	-1,00	-1,32	-1,46	-1,46	-1,42	-1,05	-0,80	-0,74
7	-0,14	-0,16	-0,16	-0,22	-0,55	-0,73	-0,96	-1,02	-0,98	-0,90	-0,70	-0,74	-0,70
8	-0,15	-0,15	-0,12	-0,16	-0,37	-0,49	-0,60	-0,61	-0,56	-0,56	-0,70	-0,74	-0,68
9	-0,11	-0,09	-0,04	-0,02	-0,14	-0,20	-0,26	-0,24	-0,33	-0,46	-0,65	-0,69	-0,66
10	-0,60	-0,49	-0,14	-0,03	+0,15	+0,02	+0,11	+0,16	+0,16	+0,16	+0,15	+0,14	+0,08
11	-0,63	-0,50	-0,20	-0,05	+0,11	+0,02	+0,10	+0,15	+0,15	+0,16	+0,15	+0,13	+0,06
12	-0,65	-0,55	-0,26	-0,16	-0,05	+0,02	+0,11	+0,16	+0,16	+0,16	+0,15	+0,14	+0,08
13	-0,66	-0,62	-0,33	-0,25	-0,10	+0,01	+0,14	+0,19	+0,20	+0,20	+0,20	+0,20	+0,16
14	-0,65	-0,84	-0,65	-0,44	-0,16	+0,04	+0,23	+0,32	+0,36	+0,39	+0,40	+0,41	+0,36
15	-0,65	-0,89	-0,95	-0,61	-0,21	+0,06	+0,31	+0,42	+0,49	+0,52	+0,54	+0,56	+0,50
16	-0,83	-1,00	-1,55	-1,33	-0,38	+0,18	+0,58	+0,73	+0,80	+0,85	+0,85	+0,88	+0,80
17	-1,11	-1,21	-2,45	-2,61	-0,35	+0,46	+0,86	+0,92	+0,89	+0,89	+0,85	+0,84	+0,91
18	-0,60	-0,47	-0,12	-0,02	+0,15	+0,02	+0,13	+0,17	+0,18	+0,17	+0,17	+0,15	+0,10
19	-0,60	-0,48	-0,10	-0,02	+0,17	+0,02	+0,14	+0,18	+0,19	+0,19	+0,18	+0,16	+0,10
20	-0,18	-0,10	0	0	0	-0,05	-0,06	-0,06	-0,26	-0,41	-0,55	-0,65	-0,64
21	-0,07	0	+0,10	+0,12	+0,07	+0,05	+0,03	-0,01	-0,24	-0,39	-0,53	-0,62	-0,60
22	-0,12	0	+0,13	+0,17	+0,15	+0,14	+0,10	+0,04	-0,21	-0,35	-0,48	-0,58	-0,56
23	-0,54	-0,35	-0,09	-0,03	0	+0,04	+0,06	+0,05	-0,02	-0,06	-0,14	-0,21	-0,26
24	-0,58	-0,40	-0,15	-0,12	-0,09	-0,03	+0,02	+0,04	-0,01	-0,04	-0,09	-0,15	-0,21
25	-0,61	-0,45	-0,21	-0,16	-0,10	0	+0,07	+0,10	+0,06	+0,05	+0,03	-0,01	-0,06
26	-0,62	-0,49	-0,25	-0,21	-0,15	-0,01	+0,08	+0,10	+0,08	+0,08	+0,04	0	-0,05

Table 2. Flap deflection  $\beta=10^\circ$ .

$\alpha^\circ$	-16,5	-13,5	-10,4	-7,4	+1,6	+7,6	+13,7	+16,7	+19,7	+21,5	+22,7	+23,6	+25,7
$c_n$	-0,50	-0,51	-0,42	-0,16	+0,47	+0,91	+1,29	+1,44	+1,52	+1,52	+1,47	+1,42	+1,02
$c_t$	+0,07	+0,04	-0,02	-0,01	+0,02	-0,04	-0,15	-0,22	-0,29	-0,25	-0,26	-0,25	-0,03
$c_m$	-0,16	-0,12	+0,01	+0,06	+0,22	+0,31	+0,40	+0,44	+0,49	+0,52	+0,52	+0,51	+0,42
Orifice location no.	$\frac{P}{q}$												
1	-0,55	-0,68	-1,50	-0,70	+0,93	+0,54	-1,12	-2,40	-3,35	-3,70	-3,95	-3,87	-0,62
2	+0,94	+0,90	+0,90	+0,79	-0,12	-1,25	-2,74	-3,57	-4,40	-4,62	-4,70	-4,52	-0,75
3	+0,65	+0,59	+0,55	+0,39	-0,54	-1,40	-2,41	-2,96	-2,99	-2,94	-2,86	-2,66	-0,75
4	+0,40	+0,31	+0,26	+0,10	-0,72	-1,41	-2,19	-2,46	-2,59	-2,46	-2,34	-2,12	-0,73
5	+0,11	+0,04	-0,01	-0,16	-0,82	-1,34	-1,87	-2,06	-2,07	-1,88	-1,68	-1,45	-0,71
6	-0,09	-0,15	-0,19	-0,30	-0,80	-1,17	-1,50	-1,65	-1,57	-1,29	-1,04	-0,85	-0,69
7	-0,20	-0,23	-0,25	-0,32	-0,68	-0,87	-1,11	-1,20	-1,10	-0,84	-0,76	-0,75	-0,67
8	-0,23	-0,24	-0,23	-0,27	-0,53	-0,64	-0,75	-0,79	-0,70	-0,71	-0,77	-0,77	-0,66
9	-0,25	-0,21	-0,18	-0,20	-0,31	-0,37	-0,42	-0,44	-0,54	-0,69	-0,74	-0,74	-0,67
10	-0,54	-0,38	-0,01	+0,10	+0,29	+0,15	+0,26	+0,30	+0,30	+0,30	+0,30	+0,30	+0,27
11	-0,51	-0,36	-0,04	+0,05	+0,20	+0,07	+0,16	+0,20	+0,19	+0,18	+0,16	+0,18	+0,14
12	-0,61	-0,45	-0,11	-0,05	0	+0,12	+0,20	+0,24	+0,21	+0,20	+0,18	+0,19	+0,15
13	-0,62	-0,52	-0,20	-0,11	+0,03	+0,14	+0,24	+0,29	+0,28	+0,28	+0,28	+0,28	+0,25
14	-0,65	-0,80	-0,50	-0,33	-0,06	+0,14	+0,31	+0,39	+0,41	+0,44	+0,46	+0,46	+0,42
15	-0,64	-0,89	-0,76	-0,50	-0,11	+0,15	+0,39	+0,48	+0,54	+0,55	+0,59	+0,59	+0,54
16	-0,77	-1,06	-1,45	-1,17	-0,25	+0,28	+0,65	+0,78	+0,84	+0,85	+0,89	+0,89	+0,81
17	-1,00	-1,31	-3,08	-2,18	-0,16	+0,59	+0,91	+0,91	+0,86	+0,84	+0,84	+0,83	+0,94
18	-0,51	-0,35	-0,01	+0,07	+0,26	+0,14	+0,25	+0,30	+0,30	+0,28	+0,27	+0,29	+0,25
19	-0,56	-0,42	-0,29	-0,27	-0,35	-0,31	-0,31	-0,29	-0,44	-0,58	-0,67	-0,67	-0,62
20	-0,59	-0,45	-0,35	-0,34	-0,42	-0,35	-0,34	-0,30	-0,46	-0,63	-0,72	-0,73	-0,60
21	-0,30	-0,20	-0,11	-0,09	-0,10	-0,09	-0,08	-0,09	-0,32	-0,46	-0,54	-0,58	-0,54
22	-0,20	-0,04	+0,07	+0,08	+0,06	-0,01	0	0	-0,25	-0,41	-0,50	-0,53	-0,50
23	-0,46	-0,18	+0,05	+0,08	+0,10	+0,11	+0,15	+0,16	+0,08	+0,02	-0,02	-0,03	-0,06
24	-0,52	-0,26	+0,04	+0,09	+0,14	+0,18	+0,22	+0,24	+0,18	+0,15	+0,13	+0,12	+0,09
25	-0,55	-0,32	+0,10	+0,23	+0,34	+0,40	+0,44	+0,45	+0,41	+0,40	+0,39	+0,38	+0,36
26	-0,55	-0,36	+0,11	+0,31	+0,56	+0,66	+0,70	+0,71	+0,69	+0,68	+0,68	+0,67	+0,66

Table 3. Flap deflection  $\beta=19^\circ$ .

$\alpha^\circ$	-16.5	-13.5	-10.4	-7.4	-4.4	+1.6	+7.6	+13.7	+16.7	+19.7	+21.0	+22.7	+24.4	+25.7
$c_n$	-0.39	-0.48	-0.22	+0.02	+0.28	+0.75	+1.14	+1.55	+1.74	+1.79	+1.80	+1.20	+1.12	+1.11
$c_t$	+0.08	+0.04	+0.01	+0.04	+0.06	+0.05	-0.02	-0.14	-0.24	-0.31	-0.32	-0.16	-0.14	+0.05
$c_m$	-0.09	-0.09	+0.10	+0.18	+0.24	+0.37	+0.45	+0.55	+0.60	+0.62	+0.62	+0.48	+0.48	+0.51
Orifice location no.	$\frac{P}{q}$													
1	-0.47	-0.66	-1.43	-0.50	+0.30	+0.94	+0.37	-1.51	-2.92	-4.10	-4.60	-3.15	-3.22	-0.60
2	+0.95	+0.94	+0.91	+0.75	+0.52	-0.27	-1.45	-3.00	-3.99	-5.17	-5.35	-3.94	-3.70	-0.69
3	+0.65	+0.60	+0.55	+0.33	+0.05	-0.66	-1.56	-2.61	-3.12	-3.35	-3.47	-2.05	-1.74	-0.69
4	+0.39	+0.33	+0.25	+0.04	-0.23	-0.85	-1.55	-2.36	-2.69	-2.90	-2.96	-1.38	-0.97	-0.68
5	+0.10	+0.04	-0.04	-0.22	-0.45	-0.94	-1.46	-1.97	-2.25	-2.35	-2.36	-0.60	-0.50	-0.67
6	-0.11	-0.15	-0.22	-0.36	-0.55	-0.91	-1.29	-1.62	-1.81	-1.81	-1.80	-0.51	-0.48	-0.66
7	-0.22	-0.24	-0.28	-0.40	-0.52	-0.80	-1.00	-1.25	-1.36	-1.32	-1.26	-0.52	-0.49	-0.65
8	-0.27	-0.25	-0.26	-0.35	-0.45	-0.66	-0.75	-0.90	-0.96	-0.91	-0.84	-0.55	-0.51	-0.64
9	-0.32	-0.23	-0.22	-0.29	-0.34	-0.46	-0.52	-0.62	-0.65	-0.62	-0.62	-0.57	-0.55	-0.65
10	-0.50	-0.32	+0.08	+0.16	+0.24	+0.36	+0.28	+0.35	+0.40	+0.42	+0.44	+0.35	+0.36	+0.37
11	-0.48	-0.35	+0.05	+0.11	+0.16	+0.28	+0.19	+0.28	+0.33	+0.32	+0.33	+0.25	+0.26	+0.27
12	-0.60	-0.41	+0.03	+0.07	+0.08	+0.09	+0.21	+0.28	+0.33	+0.32	+0.33	+0.25	+0.27	+0.26
13	-0.60	-0.50	-0.09	-0.02	+0.02	+0.13	+0.22	+0.32	+0.37	+0.39	+0.39	+0.33	+0.35	+0.35
14	-0.64	-0.80	-0.40	-0.26	-0.16	+0.02	+0.20	+0.37	+0.45	+0.49	+0.51	+0.47	+0.50	+0.50
15	-0.61	-0.95	-0.64	-0.44	-0.29	-0.03	+0.22	+0.44	+0.54	+0.60	+0.62	+0.58	+0.61	+0.60
16	-0.73	-1.10	-1.42	-1.10	-0.80	-0.14	+0.36	+0.70	+0.82	+0.87	+0.90	+0.86	+0.90	+0.85
17	-0.91	-1.33	-3.05	-1.94	-1.10	0	+0.66	+0.91	+0.90	+0.83	+0.79	+0.85	+0.85	+0.95
18	-0.60	-0.36	-0.16	-0.16	-0.17	-0.13	-0.12	-0.08	-0.04	+0.01	+0.03	-0.07	-0.05	-0.10
19	-0.75	-0.41	-0.39	-0.49	-0.59	-0.75	-0.68	-0.74	-0.69	-0.61	-0.61	-0.79	-0.76	-0.85
20	-0.81	-0.38	-0.39	-0.54	-0.71	-0.92	-0.78	-0.81	-0.72	-0.60	-0.57	-0.80	-0.78	-0.79
21	-0.56	-0.30	-0.17	-0.17	-0.17	-0.22	-0.18	-0.19	-0.19	-0.27	-0.36	-0.50	-0.50	-0.51
22	-0.40	-0.23	-0.15	-0.13	-0.06	+0.01	-0.04	+0.01	+0.01	-0.16	-0.27	-0.42	-0.42	-0.46
23	-0.44	-0.10	+0.10	+0.13	+0.15	+0.20	+0.23	+0.28	+0.30	+0.25	+0.22	+0.10	+0.11	+0.11
24	-0.50	-0.18	+0.23	+0.26	+0.27	+0.32	+0.35	+0.40	+0.44	+0.40	+0.39	+0.30	+0.31	+0.32
25	-0.54	-0.26	+0.34	+0.49	+0.56	+0.60	+0.65	+0.67	+0.69	+0.66	+0.66	+0.61	+0.63	+0.65
26	-0.54	-0.30	+0.25	+0.46	+0.68	+0.90	+0.95	+0.94	+0.95	+0.94	+0.94	+0.91	+0.93	+0.94

Table 4. Flap deflection  $\beta=34^\circ$ .

$\alpha^\circ$	-16.5	-13.5	-10.4	-7.4	-4.4	+1.6	+7.6	+13.7	+16.7	+19.7	+20.4	+22.7	+24.4	+25.7
$c_n$	-0.44	-0.34	+0.16	+0.42	+0.62	+1.14	+1.52	+1.93	+2.11	+2.08	+2.04	+1.29	+1.28	+1.27
$c_t$	+0.08	+0.09	+0.10	+0.14	+0.15	+0.14	+0.05	-0.07	-0.17	-0.25	-0.26	-0.07	-0.06	+0.13
$c_m$	-0.12	+0.03	+0.29	+0.39	+0.44	+0.59	+0.65	+0.76	+0.79	+0.77	+0.77	+0.58	+0.57	+0.61
Orifice location no.	$\frac{P}{q}$													
1	-0.42	-0.70	-1.05	-0.14	+0.55	+0.91	+0.05	-2.08	-3.65	-4.72	-4.95	-3.20	-3.20	-0.62
2	+0.82	+0.91	+0.85	+0.67	+0.38	-0.50	-1.78	-3.40	-4.71	-5.31	-5.15	-3.75	-3.36	-0.65
3	+0.64	+0.59	+0.46	+0.21	-0.10	-0.87	-1.79	-2.90	-3.30	-3.55	-3.56	-1.88	-1.55	-0.65
4	+0.39	+0.31	+0.16	-0.07	-0.37	-1.04	-1.75	-2.58	-2.95	-3.06	-3.03	-1.19	-0.80	-0.65
5	+0.11	+0.03	-0.12	-0.34	-0.59	-1.11	-1.64	-2.15	-2.46	-2.47	-2.41	-0.54	-0.48	-0.65
6	-0.09	-0.17	-0.30	-0.47	-0.68	-1.09	-1.45	-1.81	-2.00	-1.93	-1.84	-0.50	-0.48	-0.65
7	-0.20	-0.28	-0.37	-0.50	-0.66	-0.96	-1.14	-1.42	-1.55	-1.42	-1.30	-0.50	-0.49	-0.65
8	-0.23	-0.27	-0.37	-0.48	-0.60	-0.84	-0.93	-1.10	-1.17	-1.01	-0.90	-0.52	-0.51	-0.66
9	-0.25	-0.26	-0.37	-0.46	-0.56	-0.71	-0.76	-0.86	-0.92	-0.79	-0.75	-0.56	-0.55	-0.70
10	-0.45	-0.14	+0.24	+0.29	+0.31	+0.42	+0.32	+0.39	+0.43	+0.44	+0.44	+0.40	+0.40	+0.40
11	-0.51	-0.19	+0.19	+0.25	+0.31	+0.40	+0.35	+0.41	+0.45	+0.45	+0.45	+0.42	+0.44	+0.41
12	-0.61	-0.23	+0.20	+0.22	+0.21	+0.24	+0.35	+0.41	+0.45	+0.45	+0.45	+0.43	+0.44	+0.41
13	-0.60	-0.34	+0.12	+0.14	+0.18	+0.28	+0.35	+0.44	+0.49	+0.49	+0.49	+0.45	+0.47	+0.45
14	-0.63	-0.71	-0.21	-0.12	-0.02	+0.14	+0.30	+0.45	+0.53	+0.55	+0.56	+0.53	+0.56	+0.54
15	-0.61	-0.93	-0.43	-0.30	-0.15	+0.09	+0.31	+0.51	+0.60	+0.64	+0.66	+0.62	+0.65	+0.61
16	-0.70	-1.15	-1.19	-0.87	-0.56	+0.03	+0.46	+0.76	+0.85	+0.88	+0.90	+0.86	+0.90	+0.85
17	-0.79	-1.40	-2.52	-1.45	-0.76	+0.20	+0.75	+0.91	+0.85	+0.74	+0.74	+0.83	+0.82	+0.94
18	-0.52	-0.59	-0.95	-1.20	-1.41	-1.73	-1.56	-1.65	-1.65	-1.10	-1.00	-0.91	-0.95	-1.07
19	-0.53	-0.50	-0.95	-1.24	-1.47	-1.85	-1.58	-1.66	-1.65	-0.96	-0.85	-0.89	-0.90	-0.95
20	-0.49	-0.35	-0.60	-0.86	-1.06	-1.50	-1.13	-1.28	-1.31	-0.81	-0.75	-0.81	-0.80	-0.84
21	-0.48	-0.31	-0.35	-0.36	-0.36	-0.32	-0.36	-0.29	-0.27	-0.45	-0.47	-0.51	-0.48	-0.56
22	-0.46	-0.33	-0.32	-0.28	-0.24	-0.12	-0.20	-0.08	0	-0.34	-0.39	-0.41	-0.40	-0.49
23	-0.44	+0.10	+0.30	+0.30	+0.32	+0.40	+0.40	+0.46	+0.50	+0.41	+0.39	+0.35	+0.35	+0.34
24	-0.50	+0.09	+0.56	+0.55	+0.54	+0.59	+0.60	+0.65	+0.66	+0.62	+0.61	+0.58	+0.59	+0.59
25	-0.51	-0.01	+0.58	+0.85	+0.88	+0.88	+0.88	+0.88	+0.90	+0.88	+0.87	+0.86	+0.87	+0.88
26	-0.50	-0.10	+0.31	+0.68	+0.98	+1.00	+1.00	+1.00	+1.00	+0.99	+0.99	+0.99	+1.00	+1.00

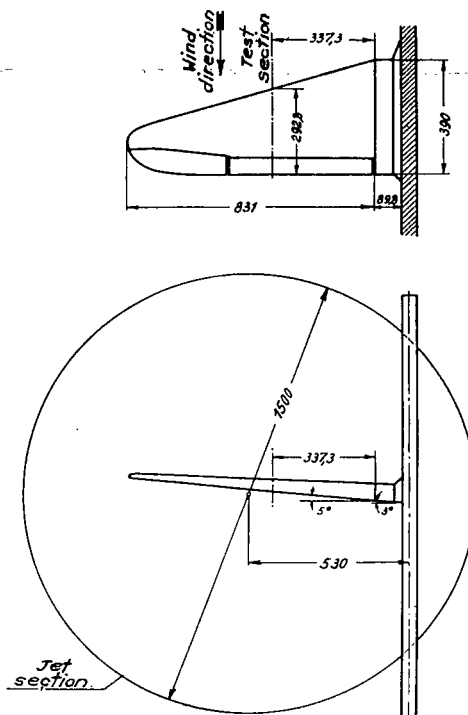
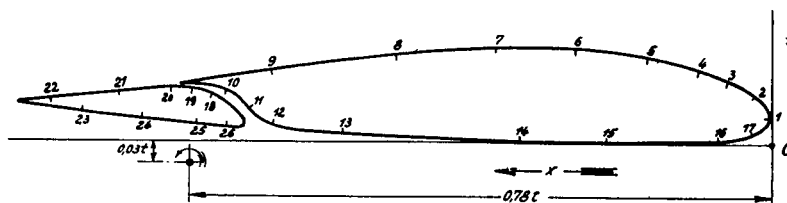


Figure 1.- Arrangement in free jet, plan form and dihedral of model wing.

Orifice location	1	2	3	4	5	6	7	8	9	10	11	12	13	14	15	16	17
x	0	2.22	5.91	9.90	16.50	25.31	36.74	49.26	65.75	71.59	68.95	65.79	54.38	33.07	21.89	7.10	2.56

Orifice location	18	19	20	21	22	23	24	25	26
x	74.05	76.95	79.9	86.10	95.0	90.83	83.23	75.78	72.23



x	0	1.25	2.5	5.0	7.5	10.0	15.0	20.0	25.0	30.0	40.0	50.0	60.0	64.45	66.62	68.65	70.0	71.8	73.8	76.2	77.9	78.67	
y <sub>0</sub>	3.42	5.94	7.87	8.57	9.70	10.52	11.78	12.53	12.98	13.08	12.81	11.81	10.52		9.08								7.65
y <sub>u</sub>	3.42	1.84	1.17	0.75	0.38	0.14	-0.03	-0.07	0	0.10	0.44	0.85	1.37	1.80	2.05	3.24	4.44	6.08	7.24	7.68	7.68	7.65	

Main airfoil.

x	70.59	70.82	71.80	71.80	72.2	72.9	73.7	80	81.6	82.0	86.0	89.0
y <sub>0</sub>	2.63	3.71	4.77	5.87	6.93	7.36	7.57		7.28	6.25	5.74	5.40
y <sub>u</sub>	2.43	2.08	1.98		2.22		2.63		3.72	4.67	5.12	

Flap.

Figure 2.- Profile of investigated wing section. Orifices were located at points 1-26.

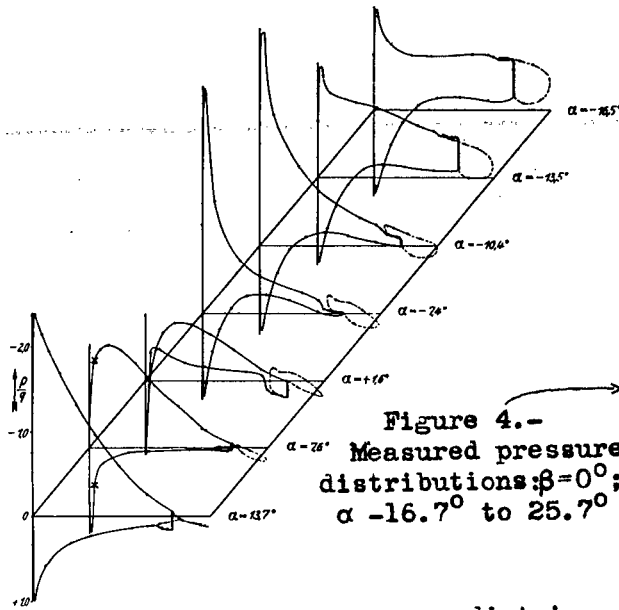


Figure 3.- Measured pressure distributions:  $\beta=0^\circ$ ,  $\alpha=-16.5^\circ$  to  $13.7^\circ$ . The flap pressure distribution is indicated by dotted line.

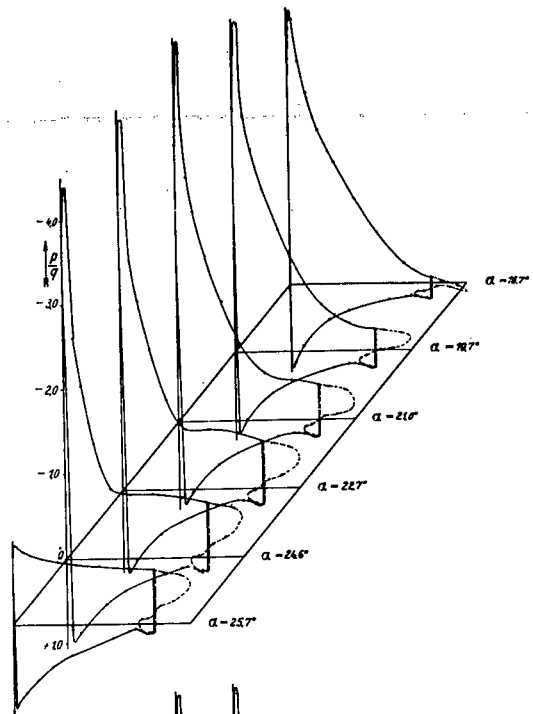


Figure 4.- Measured pressure distributions:  $\beta=0^\circ$ ;  $\alpha=-16.7^\circ$  to  $25.7^\circ$

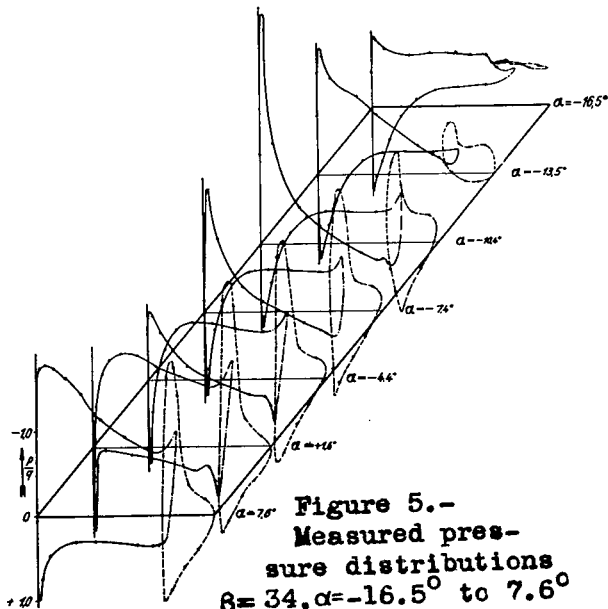


Figure 5.- Measured pressure distributions  $\beta=34^\circ$ ,  $\alpha=-16.5^\circ$  to  $7.6^\circ$ . The test points of the flap are so drawn that their distances from the nose of the section corresponds to the values given in fig. 2. At the trailing edge of the main wing the pressure distribution is drawn dotted to indicate that the curve was here not drawn thru test points and is only qualitatively correct.

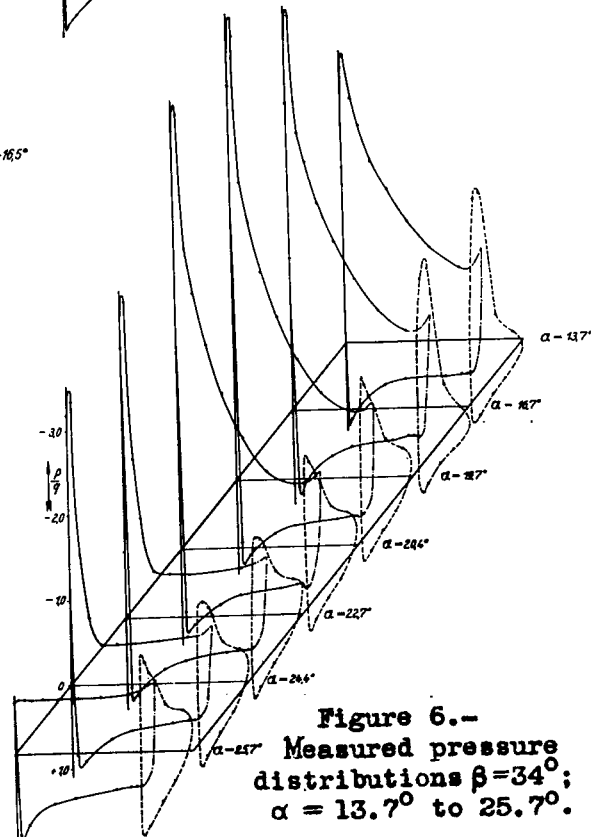


Figure 6.- Measured pressure distributions  $\beta=34^\circ$ ;  $\alpha=13.7^\circ$  to  $25.7^\circ$ .

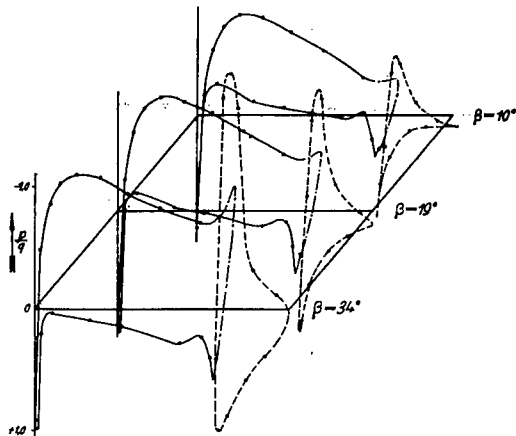


Figure 8.- Measured pressure distributions:  $\alpha = 1.6^\circ$   
 $\beta = 10^\circ, 19^\circ$  and  $34^\circ$ .

Figure 7.- Flap pressures for  $\beta = 34^\circ$   
 as functions of  $\alpha$ .



Figure 10.- Stream line picture of slot flow (flow in closed water channel), Reynolds Number about  $2 \times 10^5$ . Slot inlet is somewhat widened as compared with that of fig. 2,  $\alpha = 4^\circ, \beta = 10^\circ$ .

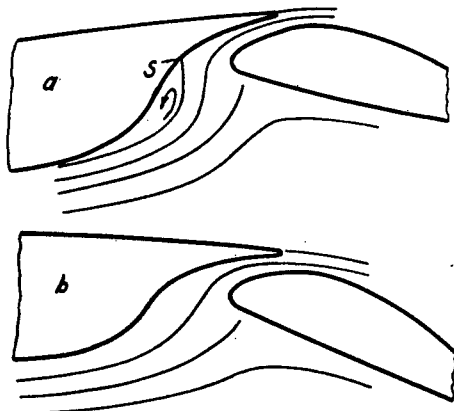


Figure 12.- Sketch of slot flow, a for  $\alpha < 3^\circ$ , b for  $\alpha > 5^\circ$ . Flap setting  $34^\circ$ .

Orifice location		
18	o	
19	•	
20	•	
21	o	
22	x	
23	•	
24	+	
25	•	
26	+	

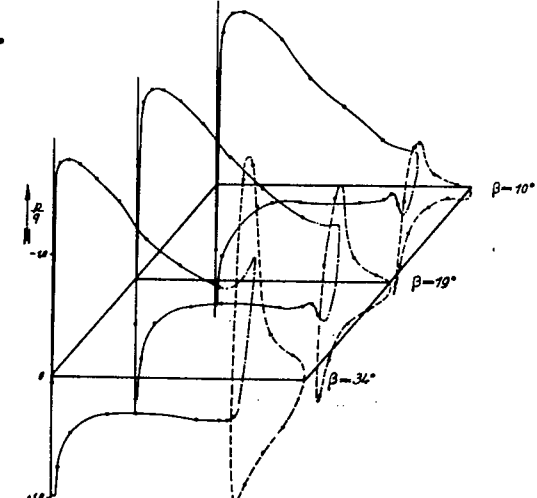
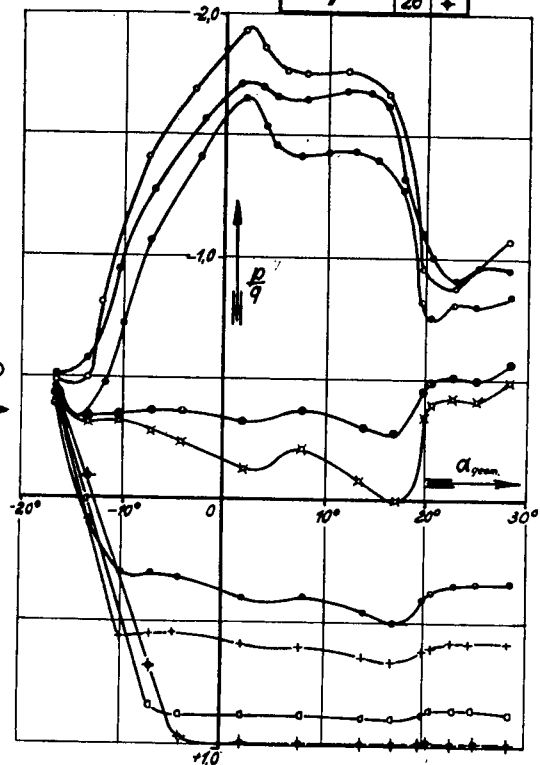
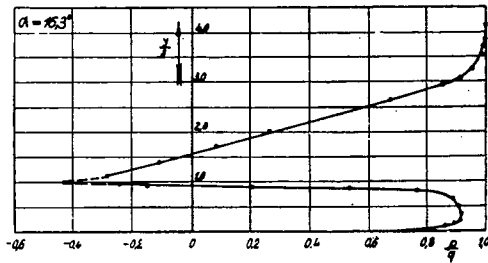
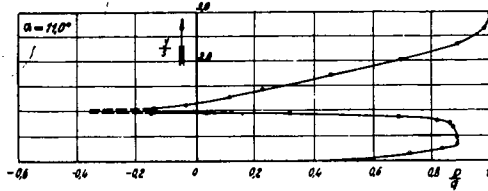
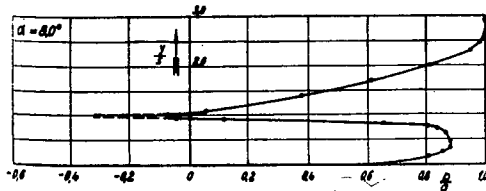
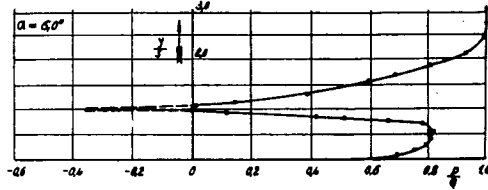
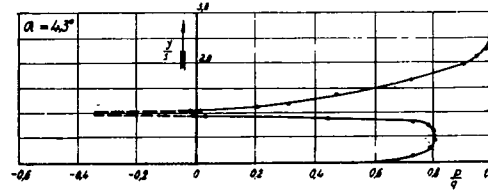
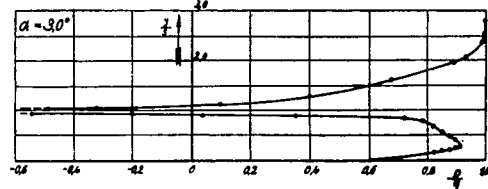
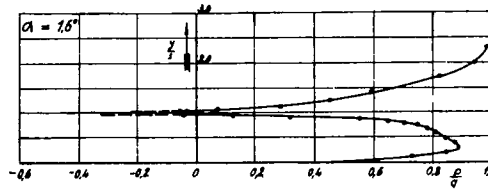
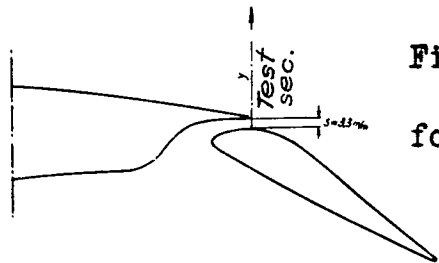


Figure 9.- Measured pressure distributions:  $\alpha = 7.6^\circ, \beta = 10^\circ, 19^\circ$   
 and  $34^\circ$ .

Figure 11.- Total pressure measurements at slot exit for a flap deflection  $\beta=34^\circ$ .



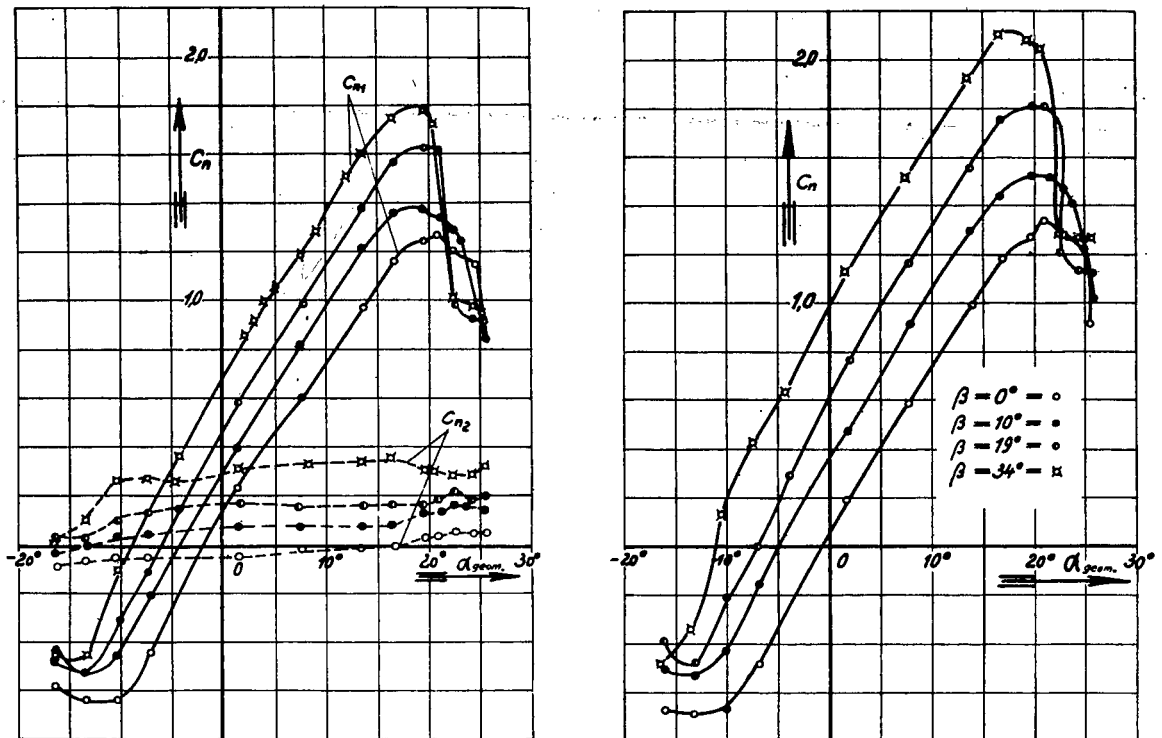


Figure 13.- Normal force coefficient as a function of angle of attack,  $C_n$  = coefficient of entire wing section,  $C_{n1}$  = coefficient of main wing section,  $C_{n2}$  = coefficient of flap section.

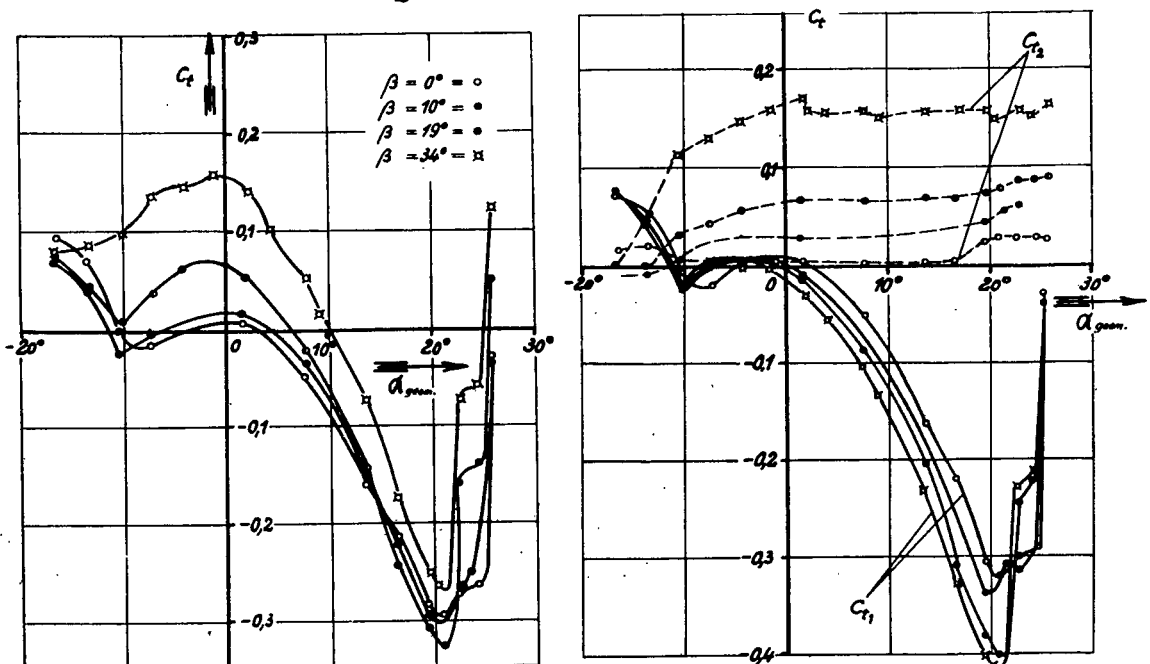


Figure 14.- Tangential force coefficient as function of angle of attack,  $C_t$  = coefficient of entire wing section,  $C_{t1}$  = coefficient of main wing section,  $C_{t2}$  = coefficient of flap section.

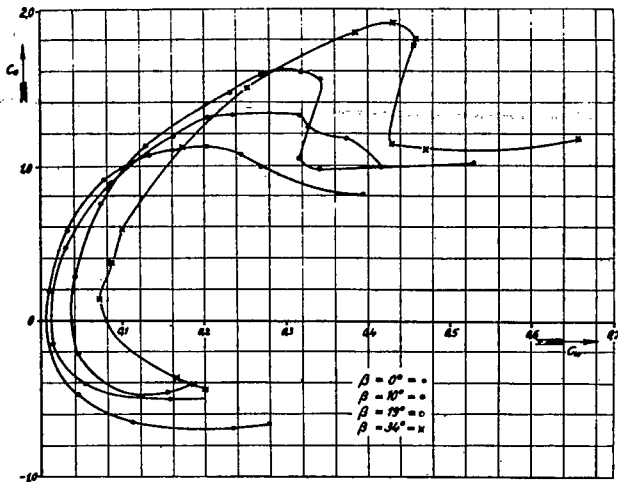


Figure 15.- Polars of investigated wing section.

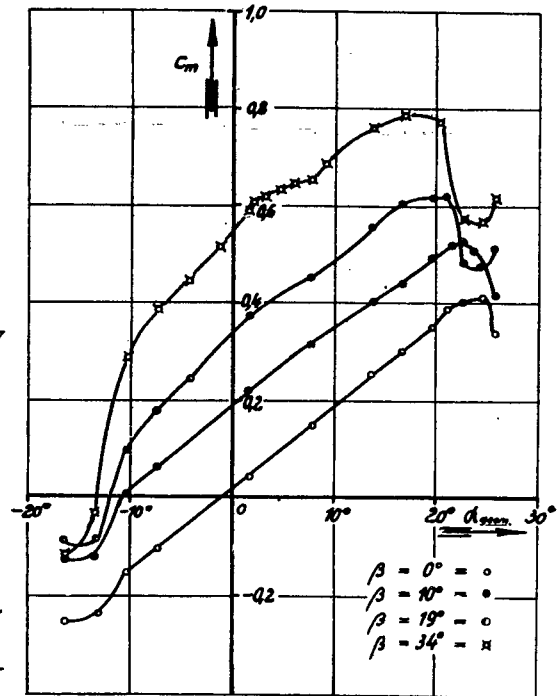


Figure 16.- Pitching moment coefficients of wing section.

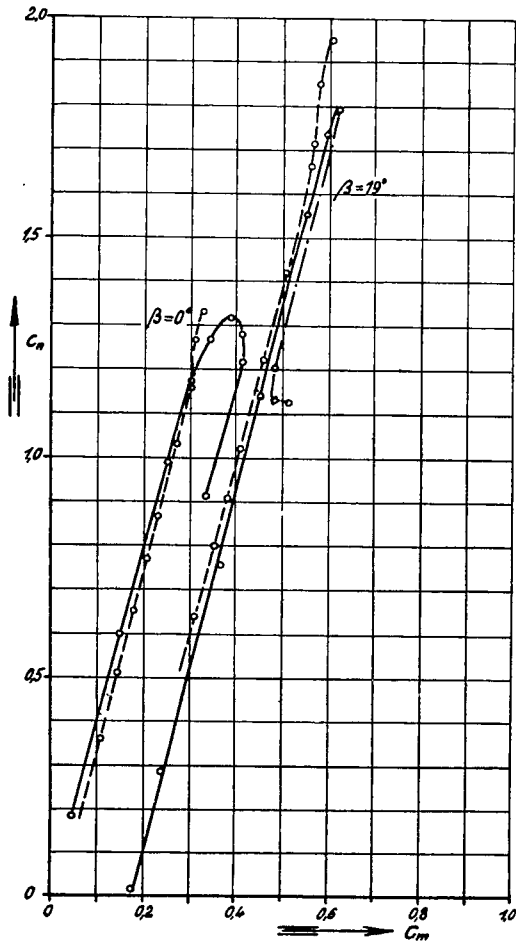


Figure 19.- Comparison of the coefficients obtained by integration of the wind tunnel and flight tests measurements. The continuous curve refers to the wind tunnel test while the dotted curve to the flight test.

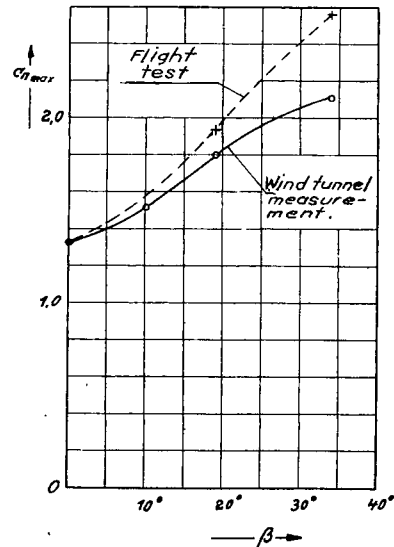


Figure 20.- Comparison of maximum normal force coefficient values from the wind tunnel and flight tests.

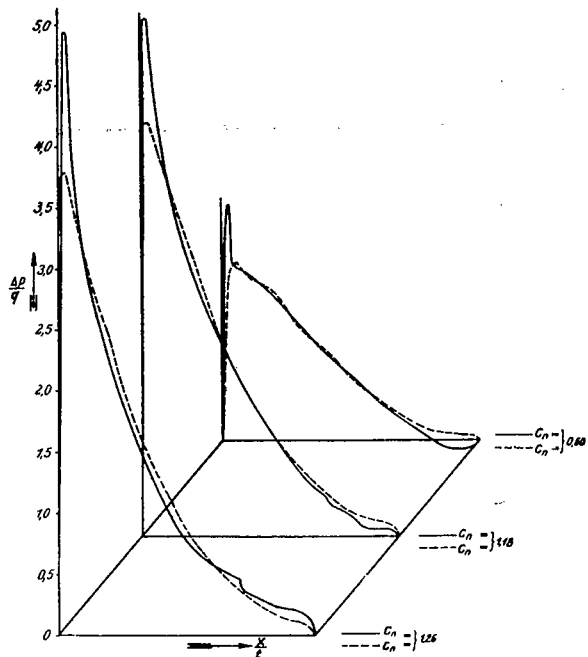


Figure 17.- Comparison of pressure distributions measured in the wind tunnel at  $\beta = 0^\circ$  with the corresponding pressure distributions obtained from the flight test. The ordinates give the algebraic sum of the pressures on the upper and lower surfaces. The continuous curve corresponds to the wind tunnel test and the dotted curve to the flight test.

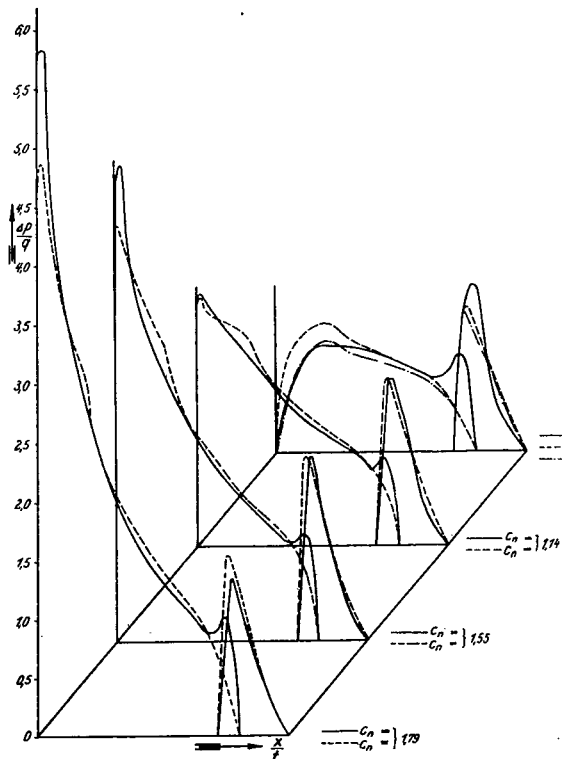


Figure 18.- Comparison of pressure distributions measured in wind tunnel at  $\beta = 19^\circ$  with the corresponding pressure distributions obtained from the flight test. The ordinates give the algebraic sum of the pressure on the upper and lower surfaces. The continuous curve corresponds to the wind tunnel test and the dotted curve to the flight test. The dot-dash curve represents a pressure resultant distribution for which Kiel gives a value of  $C_n = 0.66$ .

NASA Technical Library



3 1176 01440 6657